The Journal of Chemical Physics

RESEARCH ARTICLE | JULY 06 2022

Permutation invariant polynomial neural network based diabatic ansatz for the (*E* + *A*) × (*e* + *a*) Jahn–Teller and Pseudo-Jahn–Teller systems

Yafu Guan ; David R. Yarkony ; Dong H. Zhang

J. Chem. Phys. 157, 014110 (2022)
https://doi.org/10.1063/5.0096912
CHORUS

AIP Publishing

The Journal of Chemical Physics ARTICLE scitation.org/journal/jcp

Permutation invariant polynomial neural network based diabatic ansatz for the $(E+A)\times(e+a)$ Jahn–Teller and Pseudo-Jahn–Teller systems

Cite as: J. Chem. Phys. 157, 014110 (2022); doi: 10.1063/5.0096912
Submitted: 23 April 2022 • Accepted: 21 June 2022 •
Published Online: 6 July 2022

Yafu Guan,[1,a] David R. Yarkony,[2,b] and Dong H. Zhang[1,c]

AFFILIATIONS

[1] State Key Laboratory of Molecular Reaction Dynamics and Center for Theoretical Computational Chemistry, Dalian Institute of Chemical Physics, Chinese Academy of Sciences, Dalian 116023, People's Republic of China
[2] Department of Chemistry, Johns Hopkins University, Baltimore, Maryland 21218, USA

[a] Electronic mail: guanyf@dicp.ac.cn
[b] Electronic mail: yarkony@jhu.edu
[c] Author to whom correspondence should be addressed: zhangdh@dicp.ac.cn

ABSTRACT

In this work, the permutation invariant polynomial neural network (PIP-NN) approach is employed to construct a quasi-diabatic Hamiltonian for system with non-Abelian symmetries. It provides a flexible and compact NN-based diabatic ansatz from the related approach of Williams, Eisfeld, and co-workers. The example of H_3^+ is studied, which is an $(E+A)\times(e+a)$ Jahn–Teller and Pseudo-Jahn–Teller system. The PIP-NN diabatic ansatz is based on the symmetric polynomial expansion of Viel and Eisfeld, the coefficients of which are expressed with neural network functions that take permutation-invariant polynomials as input. This PIP-NN-based diabatic ansatz not only preserves the correct symmetry but also provides functional flexibility to accurately reproduce *ab initio* electronic structure data, thus resulting in excellent fits. The adiabatic energies, energy gradients, and derivative couplings are well reproduced. A good description of the local topology of the conical intersection seam is also achieved. Therefore, this diabatic ansatz completes the PIP-NN based representation of DPEM with correct symmetries and will enable us to diabatize even more complicated systems with complex symmetries.

I. INTRODUCTION

The study of non-adiabatic chemical processes involving more than one adiabatic state has become a frontier of theoretical chemistry.[1] A better understanding of these non-adiabatic processes requires a full quantum treatment, and it is far more advantageous to work within a diabatic representation than an adiabatic representation to study non-adiabatic processes.[2] For polyatomic molecules, rigorous diabatic representations do not exist.[3–5] To be more precise, the term quasi-diabatic should be used. However, for simplicity, the attribute *quasi* will be omitted below.

A diabatic representation is given by a diabatic potential energy matrix (DPEM), whose elements are continuous and smooth functions of the nuclear coordinates. By diagonalizing the DPEM, Adiabatic-to-Diabatic (AtD) transformation can be obtained, and adiabatic energies, energy gradients, and derivative couplings can then be evaluated. Due to the non-uniqueness of a diabatic representation, there are a variety of methods of diabatization. According to the type of information used, the methods of diabatization can be grouped into several categories: derivative-based methods, property-based methods, methods based on electronic wavefunctions, and diabatization by ansatz. In principle, the derivative-based methods are the most accurate, as the derivative couplings are directly used to diabatize the electronic states. Some derivative-based methods reported in the literature include (i) solving the Poisson equation,[6,7] (ii) the Shepard interpolation,[8–10] and (iii) line integral methods.[11–13] On the other hand, the basic idea for property-based methods is that molecular properties in diabatic bases should be smooth and continuous functions of the nuclear coordinates. One of the most frequently used molecular properties is the electric dipole

moment, such as in the generalized Mulliken–Hush method[14,15] or the Werner–Meyer dipole method.[16] Other properties used in diabatization include quadrupole[17] and angular momentum.[18] Methods that used more than one property have also been reported.[19,20] Alternatively, the diabatic states can be constructed directly based on the information of electronic wavefunctions. The idea of configurational uniformity is widely accepted in such methods,[21,22] the basic principle behind which is that the dominant character of a diabatic state can be expressed as a single configuration state function (CSF) or a linear combination of CSFs, which is preserved as the configurational space evolves. Block-diagonalization is another similar method that is widely used,[23–26] where the adiabatic wavefunctions are expanded as linear combinations of diabatic basis states and each diabatic basis state is a linear combination of reference CSFs.

Diabatization by ansatz is also widely used due to its simplicity, in which only the adiabatic energies are fit with a physically inspired DPEM model (ansatz). An exemplary application of diabatization by ansatz is the vibronic coupling approach,[27] in which the DPEM is expressed with only a low (first or second) order Taylor expansion of the normal coordinates around a reference geometry. In recent years, higher-order expansions have been introduced for the vibronic coupling approach to represent more extended regions of the potential energy surfaces (PESs).[28–36] More recently, artificial neural networks (NNs) have been incorporated into the ansatz to make vibronic coupling models more flexible.[37–40]

Hybrid methods have also been developed, including the hybrid method of block-diagonalization and diabatization by ansatz.[41] Zhu and Yarkony proposed a Fitting-and-Diabatizing (FaD) method,[42–45] which can be viewed as a hybrid method of derivative-based method and diabatization by ansatz. In this method, the DPEM is expressed with symmetrized functional form, the parameters of which are determined by reproducing *ab initio* energies, energy gradients and derivative couplings. During the fitting-and-diabatizing procedure, the residual derivative couplings can be determined and used to assess the quality of the diabatization. Therefore, this method can ultimately provide an accurate, quantifiable quasi-diabatic representation.

No matter which diabatization method is employed, in order to represent the DPEM analytically, correct symmetry adaptation must be applied. The point group symmetry is often inadequate for describing the breaking and forming of chemical bonds. The appropriate symmetry group describing a molecular system in the entire configuration space is the complete nuclear permutation and inversion (CNPI) group.[46] The electronic Hamiltonian commutes with the CNPI group, i.e., CNPI group operators leave the electronic Hamiltonian invariant, the diabatic states of the electronic Hamiltonian will thus carry corresponding irreducible representations of the CNPI group. If the diabatic states carry one-dimensional irreducible representations, i.e., only Abelian symmetries are involved, then the DPEM element H_{ij}^d will transform as a one-dimensional irreducible representation according to the following equation:

$$irred(\mathbf{\Psi}_i^d) \otimes irred(\mathbf{\Psi}_j^d), \tag{1}$$

where $irred(\mathbf{\Psi}_i^d)$ denotes the irreducible representation carried by the diabatic state $\mathbf{\Psi}_i^d$.

The representation of DPEM with Abelian symmetries has been fully addressed. Zhu and Yarkony proposed a general projection operator method generating symmetry-adapted polynomial (SAP) expansions to represent the DPEM elements.[42–45] Artificial neural networks have been introduced to represent DPEM, which include the first attempts of Lenzen and Manthe.[47,48] More recent efforts include the use of permutation-invariant polynomials[49] (PIPs) and artificial neural networks.[50,51] The PIPs can be viewed as a special case of the projection operator method. The basic coordinates employed in PIPs are the internuclear distances, and the corresponding projection operator is that of the totally symmetric irreducible representation. The PIP-NN method is widely adopted in the construction of adiabatic PESs for polyatomic molecules in the gas phase[52–54] and for the interaction of small molecules with (frozen) surfaces.[55] The PIP-NN PESs based on high-level *ab initio* calculations have been proven very accurate in molecular spectroscopy and reaction dynamics.[56,57] PIP-NN can be readily used to express totally symmetric elements of a DPEM. As for the other Abelian symmetry elements, one can still take advantage of the PIP-NN by multiplying a symmetric factor.[2,50,51]

However, when it comes to higher dimensional irreducible representations, i.e., non-Abelian groups, complications arise, as some of the DPEM elements do not transform as a one-dimensional irreducible representation. Degeneracies associated with high-dimensional irreducible representations are symmetry-required.[58] An example is provided by the two lowest electronic states in alkali metal trimers X_3 at D_{3h} geometry, which correspond to the components of an E type irreducible representation of the CNPI group $D_{3h}(\mathbf{M})$.[46,59]

Jahn–Teller (JT) effect is a long standing subject that comes with multi-dimensional degeneracies. The most studied example of the JT system is the $E \times e$ case, where the degeneracy of a doubly degenerate electronic state of E symmetry is lifted by the nuclear coordinate of the e symmetry, forming a conical intersection (CI) on the adiabatic potential energy surfaces. The conical intersection in JT systems can be reproduced by constructing a DPEM, and the vibronic coupling approach is widely adopted. In order to preserve the correct symmetry, additional relations of the expansion coefficients have to be imposed based on group theory.[28,32] Viel and Eisfeld have already expanded the Taylor series up to the sixth order for $E \times e$ JT systems.[28] An expansion involving two e symmetry modes has also been reported.[32] Similar diabatic Hamiltonian has also been developed for pseudo-Jahn–Teller (PJT) systems, where a degenerate electronic state is coupled to a nearby nondegenerate electronic state via a vibrational mode.[29,60]

The diabatic vibronic coupling models for JT and PJT systems developed by Eisfeld and co-workers have proved to be very stable and accurate, especially for describing the vicinity of a degeneracy. Recently, Eisfeld and co-workers have also introduced artificial neural networks to the vibronic coupling model to describe a more complicated electronic structure,[37,38] where the coefficients of polynomials are modulated by NN. In their most recent work, CNPI invariants were used as NN inputs rather than symmetry-adapted coordinates, with the correct symmetry being restored.[39,40] They have demonstrated that the newly developed diabatic NN model can

be very accurate, and more than 90 000 energies for five PES sheets can be well reproduced.

Considering the effectiveness of the PIP-NN approach, in this work, based on the Viel and Eisfeld expansion, we will introduce PIP-NN in the construction of a three-state diabatic Hamiltonian for H_3^+ with the FaD procedure of Zhu and Yarkony. Despite its simple electronic structure, only a few diabatizations for the three-state H_3^+ were reported in the literature, which include Kamisaka–Bian–Nobusada–Nakamura (KBNN) surface;[61] Viegas, Alijah, and Varandas surface with multi-sheeted double many-body expansion (DMBE);[62] and Adhikari and co-workers surface based on line integrals of derivative couplings.[12,63] More recently, Yin and co-workers constructed a NN-based three-state diabatic model for H_3^+, the symmetry of which is embedded in a valence bond (VB) model.[64]

The $1^1A'$, $2^1A'$, and $3^1A'$ states of H_3^+ form a $(E+A)\times(e+a)$ Jahn–Teller and pseudo-Jahn–Teller system. At D_{3h} geometry, the first and second excited states are degenerate and correspond to the two components of an E' type irreducible representation. The ground state, which is of A' symmetry, interacts with E' states via pseudo-Jahn–Teller coupling. The three internal degrees of freedom can be decomposed into $e+a$ normal modes. Our NN-based ansatz for H_3^+ is based on the polynomial expansion of Viel and Eisfeld for $(E+A)\times(e+a)$ systems,[29] the coefficients of which are expressed by NN functions with PIPs as inputs. Compared to the work of Williams, Eisfeld, and co-workers on NN based ansatz,[37–40] the main difference of our work is how NN is introduced. In their work, NN is introduced as a term of correction, the accuracy of diabatic ansatz mostly relies on the polynomial expansion, where the coefficients are taken as constants. In the present work, the coefficients of expansion are set as NN functions with PIPs inputs: NN(PIP). The dependence of DPEM on a normal mode is absorbed by NN(PIP), and the symmetry with respect to e normal modes is embedded in the polynomial expansion. With the coefficients of expansion taken as NN functions, the diabatic ansatz has a more compact form, in the sense that NN(PIP) acts as both coefficients of expansion and correction terms in the work of Williams and Eisfeld. With the coefficients of expansion taken as adjustable functions, also taking the flexibility of NN into consideration, the resulting ansatz will be more flexible. This NN-based ansatz will be employed in a FaD procedure, where the NN parameters are determined by a least-squares fitting to *ab initio* energies, energy gradients, and derivative couplings.

This paper is organized as follows: Sec. II reports the FaD procedure with PIP-NN-based ansatz. The fitting results are presented in Sec. III. Section IV summarizes and suggests future directions to be pursued.

II. METHODS

A. The PIP-NN based diabatic Hamiltonian for H_3^+

The quasi-diabatic Hamiltonian $\mathbf{H}^{\mathrm{d}}$ for H_3^+ in real representation is a 3×3 symmetric matrix whose elements are continuous functions of internal coordinates and is decomposed into following polynomial expansion up to sixth order:

$$\mathbf{H}^{\mathrm{d}}(\mathbf{R}) = \sum_{n=0}^{6}\left\{\begin{pmatrix} V_A^{(n)} & 0 & 0 \\ 0 & V_E^{(n)} & 0 \\ 0 & 0 & V_E^{(n)} \end{pmatrix} + \begin{pmatrix} 0 & 0 & 0 \\ 0 & W_{JT}^{(n)} & Z_{JT}^{(n)} \\ 0 & Z_{JT}^{(n)} & -W_{JT}^{(n)} \end{pmatrix} + \begin{pmatrix} 0 & W_{PJT}^{(n)} & -Z_{PJT}^{(n)} \\ W_{PJT}^{(n)} & 0 & 0 \\ -Z_{PJT}^{(n)} & 0 & 0 \end{pmatrix}\right\}, \tag{2}$$

where[29]

$$V^{(0)} = a_1^{(0)}, \tag{3a}$$

$$V^{(1)} = 0, \tag{3b}$$

$$V^{(2)} = a_1^{(2)}\left[x^2+y^2\right], \tag{3c}$$

$$V^{(3)} = a_1^{(3)}\left[2x^3-6xy^2\right], \tag{3d}$$

$$V^{(4)} = a_1^{(4)}\left[x^4+2x^2y^2+y^4\right], \tag{3e}$$

$$V^{(5)} = a_1^{(5)}\left[2x^5-4x^3y^2-6xy^4\right], \tag{3f}$$

$$V^{(6)} = a_1^{(6)}\left[2x^6-30x^4y^2+30x^2y^4-2y^6\right] + a_2^{(6)}\left[x^6+3x^4y^2+3x^2y^4+y^6\right], \tag{3g}$$

$$W^{(0)} = 0, \tag{4a}$$

$$W^{(1)} = \lambda_1^{(1)}x, \tag{4b}$$

$$W^{(2)} = \lambda_1^{(2)}\left[x^2-y^2\right], \tag{4c}$$

$$W^{(3)} = \lambda_1^{(3)}\left[x^3+xy^2\right], \tag{4d}$$

$$W^{(4)} = \lambda_1^{(4)}\left[x^4-6x^2y^2+y^4\right]+\lambda_2^{(4)}\left[x^4-y^4\right], \tag{4e}$$

$$W^{(5)} = \lambda_1^{(5)}\left[x^5-10x^3y^2+5xy^4\right]+\lambda_2^{(5)}\left[x^5+2x^3y^2+xy^4\right], \tag{4f}$$

$$W^{(6)} = \lambda_1^{(6)}\left[x^6-5x^4y^2-5x^2y^4+y^6\right]+\lambda_2^{(6)}\left[x^6+x^4y^2-x^2y^4-y^6\right], \tag{4g}$$

and

$$Z^{(0)} = 0, \tag{5a}$$

$$Z^{(1)} = \lambda_1^{(1)}y, \tag{5b}$$

$$Z^{(2)} = -2\lambda_1^{(2)}xy, \tag{5c}$$

$$Z^{(3)} = \lambda_1^{(3)}\left[x^2y+y^3\right], \tag{5d}$$

$$Z^{(4)} = \lambda_1^{(4)}\left[4x^3y-4xy^3\right]+\lambda_2^{(4)}\left[-2x^3y-2xy^3\right], \tag{5e}$$

$$Z^{(5)} = \lambda_1^{(5)}\left[-5x^4y+10x^2y^3-y^5\right]+\lambda_2^{(5)}\left[x^4y+2x^2y^3+y^5\right], \tag{5f}$$

$$Z^{(6)} = \lambda_1^{(6)}\left[4x^5y-4xy^5\right]+\lambda_2^{(6)}\left[-2x^5y-4x^3y^3-2xy^5\right]. \tag{5g}$$

x and y are the two components of the degenerate pair of e modes, the definition of which is following:[65]

$$x = \frac{2R_{13}^2 - R_{23}^2 - R_{12}^2}{R_{12}^2 + R_{23}^2 + R_{13}^2}, \tag{6a}$$

$$y = \frac{\sqrt{3}(R_{23}^2 - R_{12}^2)}{R_{12}^2 + R_{23}^2 + R_{13}^2}, \tag{6b}$$

where R_{ij} denotes the internuclear between two hydrogen atoms i and j. The polynomial expansions of V, W and Z are based on the work of Viel and Eisfeld on $(E+A)\times(e+a)$ Jahn–Teller and pseudo-Jahn–Teller system.[29]

In the works of Williams and Eisfeld on NN-based ansatz,[37,39] the coefficients of expansion are

$$\lambda_L(\mathbf{Q}) = \begin{cases} \lambda_L^0 \text{ (uncorrected terms)}, \\ \lambda_L^0 \cdot (1 + \eta_L^{(f)}(\mathbf{Q})) \text{ (corrected terms)}, \end{cases} \tag{7}$$

where $\mathbf{Q}$ are symmetry-adapted coordinates, λ_L^0 are constants obtained from standard nonlinear fitting procedures, and $\eta_L^{(f)}(\mathbf{Q})$ are NN functions. As can be seen, the NN functions that were introduced as terms of correction provided additional flexibility. Therefore, the accuracy of that model mostly relies on the polynomial expansion with constant coefficients (λ_L^0). However, in the present work, the coefficients $a_i^{(n)}$ and $\lambda_i^{(n)}$ are expressed with NN functions that take PIPs as input: $\mathrm{NN}_{k,i}^{(n)}(\mathrm{PIP})$, where $k = a$ or λ. The NN parameters are determined in a FaD fitting procedure. By setting the coefficients as adjustable NN functions, the resultant ansatz has a more compact form due to the absence of corrected terms. By comparison with the work of Bhattacharyya and co-workers on a similar $(E+A)\times(e+a)$ system,[60] it can be observed that the dependence of the DPEM on a symmetry coordinate is described by the NN(PIP) functions, thus the correct symmetry is preserved. Considering the high flexibility of NN functions, this ansatz is also very flexible to accurately reproduce *ab initio* data in the following FaD procedure.

The eigenvectors of $\mathbf{H^d}$ satisfy the following electronic Schrödinger equation:

$$[\mathbf{H}^{\mathrm{d}}(\mathbf{R}) - \mathbf{I}E^{a,J,(m)}(\mathbf{R})]\mathbf{d}^J(\mathbf{R}) = \mathbf{0}, \tag{8}$$

where $\mathbf{I}$ is identity matrix and $E^{a,J,(m)}$ is the corresponding eigenenergy. The superscript (m) indicates that the results come from the model Hamiltonian $\mathbf{H}^{\mathrm{d}}$, rather than *ab initio* (ab) calculations, and the superscript (a) indicates the adiabatic representation.

B. Feed-forward neural networks

In this work, a feed-forward NN is employed, which is a powerful and robust fitting tool that can, in principle, represent any real and smooth function to an accuracy consistent with the quality of the data.[66] The structure of a multilayer feed-forward NN can be denoted as R–S^1 – S^2 – ⋯ – S^M, which means that the network has R elements in the input vector and S^m neurons in layer m. In a feed-forward NN, the output of one layer becomes the input of the following layer. The input layer is denoted as the zeroth layer $(S^0 = R)$. The equations that describe the connection between layers are

$$n_i^m = \sum_{j=1}^{S^{m-1}} (w_{i,j}^m a_j^{m-1}) + b_i^m, \tag{9a}$$

$$a_i^m = f^m(n_i^m), \tag{9b}$$

where a_i^m denotes the output of neuron i in layer m, n_i^m is the net input for layer m, f^m is the transfer function, $w_{i,j}^m$ represents the element at row i and column j of the weight matrix coupling layer $m-1$ to layer m, and b_i^m denotes the bias of neuron i in layer m. Feed-forward NNs also provide closed analytical form for the gradient, thus facilitating a derivative-based diabatization.[67,68]

C. Determination of NN parameters from *ab initio* data

The nonlinear parameters $\boldsymbol{\theta}$ (weights and biases) in NN are optimized by minimizing the differences between $\mathbf{H}^{\mathrm{d}}$ determined and *ab initio* determined energies, energy gradients, and interstate couplings. The inclusion of interstate (derivative) couplings in the NN training serves to make $\mathbf{H}^{\mathrm{d}}$ diabatic in the least squares sense.[42] For *ab initio* calculations, define

$$L_0^{I,I,(ab)}(\mathbf{R}) = E^{I,(ab)}(\mathbf{R}), \tag{10a}$$

$$L_k^{I,I,(ab)}(\mathbf{R}) = \nabla_k E^{I,(ab)}(\mathbf{R}), \tag{10b}$$

$$L_k^{I,J,(ab)}(\mathbf{R}) = h_k^{I,J,(ab)}(\mathbf{R}), \tag{10c}$$

where $h_k^{I,J,(ab)}$ is the interstate coupling and k labels the gradient (coupling) components. The definition of interstate coupling is $h_k^{I,J} = f_k^{I,J}(E_J - E_I)$, where $f_k^{I,J}$ is the derivative coupling. The expressions for the $\mathbf{H}^{\mathrm{d}}$ determined (m) counterparts are

$$L_0^{I,I,(m)}(\mathbf{R}) = \mathbf{d}^I(\mathbf{R})^\dagger \mathbf{H}^{\mathrm{d}} \mathbf{d}^I(\mathbf{R}), \tag{11a}$$

$$L_k^{I,I,(m)}(\mathbf{R}) = \mathbf{d}^I(\mathbf{R})^\dagger (\nabla_k \mathbf{H}^{\mathrm{d}}) \mathbf{d}^I(\mathbf{R}), \tag{11b}$$

$$L_k^{I,J,(m)}(\mathbf{R}) = \mathbf{d}^I(\mathbf{R})^\dagger (\nabla_k \mathbf{H}^{\mathrm{d}}) \mathbf{d}^J(\mathbf{R}). \tag{11c}$$

The optimized parameters are obtained by minimizing the following performance index:

$$P(\boldsymbol{\theta}) = \frac{1}{2}\sum_{q=1}^{Q}\sum_{k}\sum_{I=1}^{N^{\mathrm{state}}}\sum_{J=I}^{N^{\mathrm{state}}}\left[L_{q,k}^{I,J,(m)} - L_{q,k}^{I,J,(ab)}\right]^2 + \frac{1}{2}t\boldsymbol{\theta}^\dagger\boldsymbol{\theta}, \tag{12}$$

where $\frac{1}{2}t\boldsymbol{\theta}^\dagger\boldsymbol{\theta}$ is the regularization term to alleviate overfitting and t is a small positive factor (10^{-6} in the present work). The index q labels different geometries, and the index k is redefined here to include both energies $(k=0)$ and gradient (coupling) components. The Levenberg–Marquardt algorithm is employed to minimize the performance index.[69] To achieve the best results, multiple trainings with different randomly generated initial parameters were performed (50 trainings in the present work), from which the optimal DPEM was chosen.

TABLE I. Properties of NN-based H^d.

Data points	2 754
Total least squares error term	38 235
Number of PIPs	6
Number of NN parameters	2 132
RMS energy error (cm^{-1})	94.8
MU energy error (cm^{-1})	61.8
RMS gradient error (%)	7.74
MU gradient error (%)	2.06

TABLE II. Energies and geometrical parameters for critical points on the ground state. Geometries are shown in three internuclear distances.

Critical point	minD_{3h}	sad$D_{\infty h}$
Ab initio energies (cm^{-1})	0.0	14 288.4
NN determined energies (cm^{-1})	5.3	14 266.0
Ab initio geometries (bohr)	1.65, 1.65, 1.65	1.54, 1.54, 3.08
NN determined geometries (bohr)	1.65, 1.65, 1.65	1.53, 1.53, 3.06

D. Electronic structure data of H_3^+

The *ab initio* calculations for H_3^+ were performed in C_s symmetry. The molecular orbitals were obtained from a state-averaged multiconfiguration self-consistent field (SA-MCSCF) treatment that averaged three $^1A'$ states with equal weights and a complete active space (two electrons, ten orbitals). The basis set used was cc-pV5Z. The dynamic correlation was incorporated using multireference configuration interaction with all single and double excitations (MR-CISD). The MR-CISD wavefunctions consist of 7395 CSFs. All electronic structure calculations reported in this work were performed using the COLUMBUS suite of electronic structure codes.[70,71] The reference energy is that of the ground state D_{3h} minimum being −1.343 589 366 6 Hartree.

The configuration space was sampled with a 3D grid spanned by following coordinates:[65]

$$\rho = \sqrt{\frac{R_{12}^2 + R_{23}^2 + R_{13}^2}{3}}, \tag{13a}$$

$$s = \sqrt{x^2 + y^2}, \tag{13b}$$

$$\phi = \arctan\left(\frac{y}{x}\right). \tag{13c}$$

The values of ρ, s, and ϕ were fixed within the range of $1.0 \le \rho \le 15.0$ bohr, $0 < s < 1$, and $0 < \phi < \pi/3$. Geometries with symmetries were excluded to avoid artificial discontinuities, which include the D_{3h} geometry ($s = 0$), collinear geometries ($s = 1$), and the C_{2v} geometries ($\phi = 0, \pi/3$). A total of 2754 geometries were assembled.

III. RESULTS AND DISCUSSION

A. Accuracy of NN-based H^d: General metrics

The NN structure used in this work was 6-30-30-32, which has two hidden layers. The transfer function in the first and second layers is hyperbolic tangent function $f(x) = \tanh(x)$; in the third layer, it is a linear function $f(x) = x$. PIPs for H_3^+ were generated by the Effective Monomial Symmetrization Approach (EMSA) program.[72] Six PIPs, including all the first, second, and third order PIPs, were used as the input of this NN. Internuclear distances in PIPs were scaled using the function $p_{ij} = \exp(-\alpha R_{ij})$, where $\alpha = 0.5$ $bohr^{-1}$. The exact form of PIPs used is as follows:

$$G_1 = p_{12} + p_{13} + p_{23}, \tag{14a}$$

$$G_2 = p_{13}p_{23} + p_{12}p_{23} + p_{12}p_{13}, \tag{14b}$$

$$G_3 = p_{12}^2 + p_{13}^2 + p_{23}^2, \tag{14c}$$

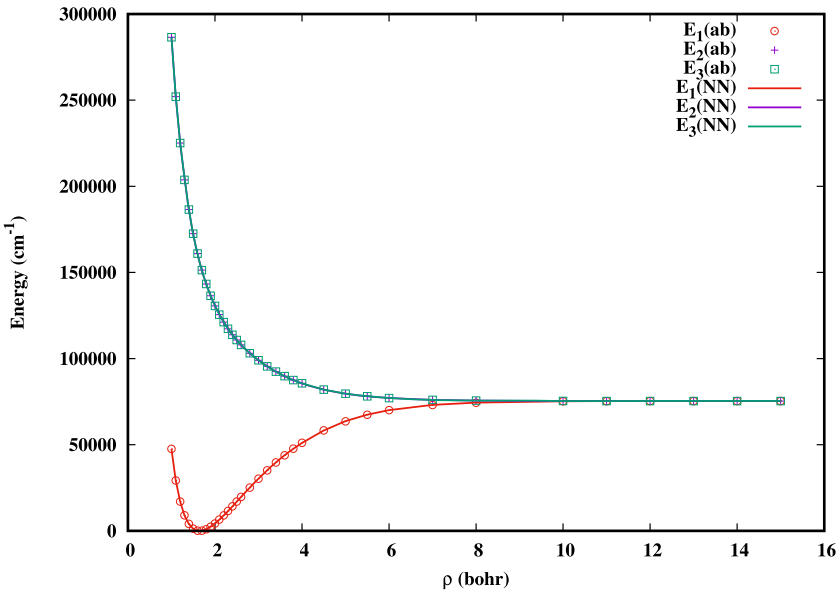

FIG. 1. Adiabatic energies as functions of ρ at D_{3h} geometries ($s = 0$). *Ab initio* energies are shown as symbols, and energies from the NN model are shown as lines.

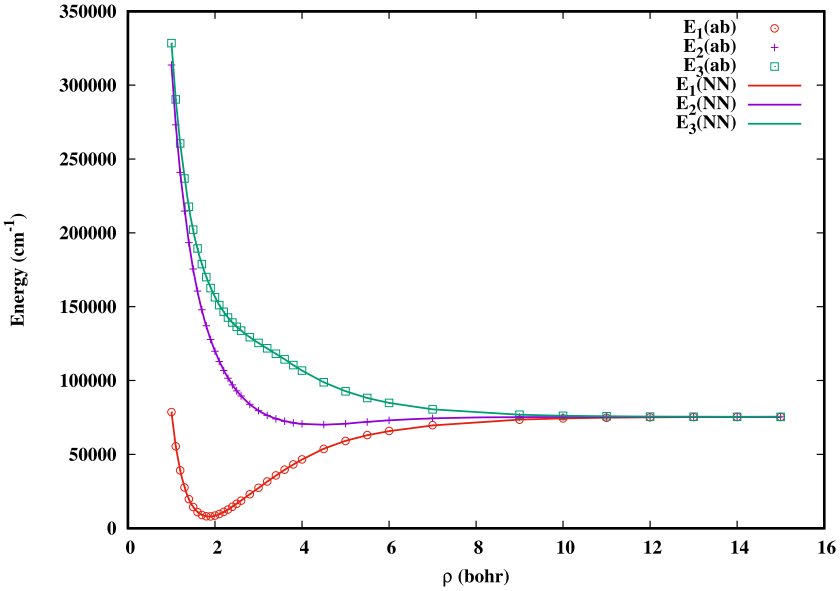

FIG. 2. Adiabatic energies as functions of ρ at C_{2v} geometries ($s = 0.5$ and $\phi = \pi/3$). *Ab initio* energies are shown as symbols, and energies from the NN model are shown as lines.

$$G_4 = p_{12}p_{13}p_{23}, \tag{14d}$$

$$G_5 = p_{13}p_{23}^2 + p_{13}^2p_{23} + p_{12}p_{23}^2 + p_{12}p_{13}^2 + p_{12}^2p_{23} + p_{12}^2p_{13}, \tag{14e}$$

$$G_6 = p_{12}^3 + p_{13}^3 + p_{23}^3. \tag{14f}$$

Each NN output component corresponds to an independent coefficient $(a_i^{(n)}, \lambda_i^{(n)})$ in Eqs. (3)–(5). Both JT and PJT terms have 16 independent coefficients, thus giving rise to a total of 32 NN output components.

Key results describing the NN fit are summarized in Table I. The reproduction of energies and energy gradients is reported in root mean square (rms) error and mean-unsigned (MU) error. The overall accuracy of the fit is quite satisfactory: the rms (MU) error for all energy terms is 94.8 (61.8) cm^{-1}, and the rms (MU) error of all energy gradients is 7.74 (2.06) %. In addition, the ratio between the number of least square error terms and the number of NN parameters is as large as 38 235/2132, which indicates the NN-based ansatz is well-suited for describing H_3^+ system and a small size of NN is sufficient to achieve good fitting results.

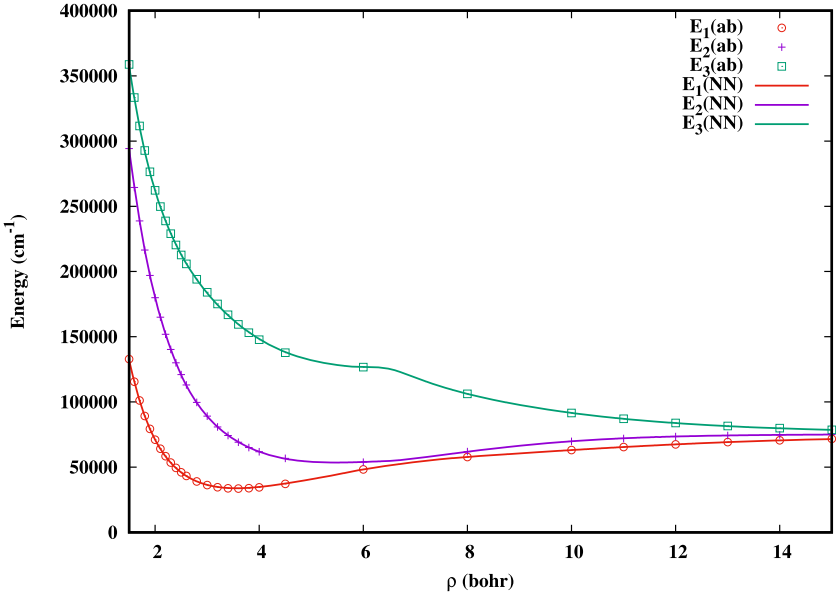

FIG. 3. Adiabatic energies as functions of ρ at collinear geometries ($s = 1$ and $\phi = \pi/6$). *Ab initio* energies are shown as symbols, and energies from the NN model are shown as lines.

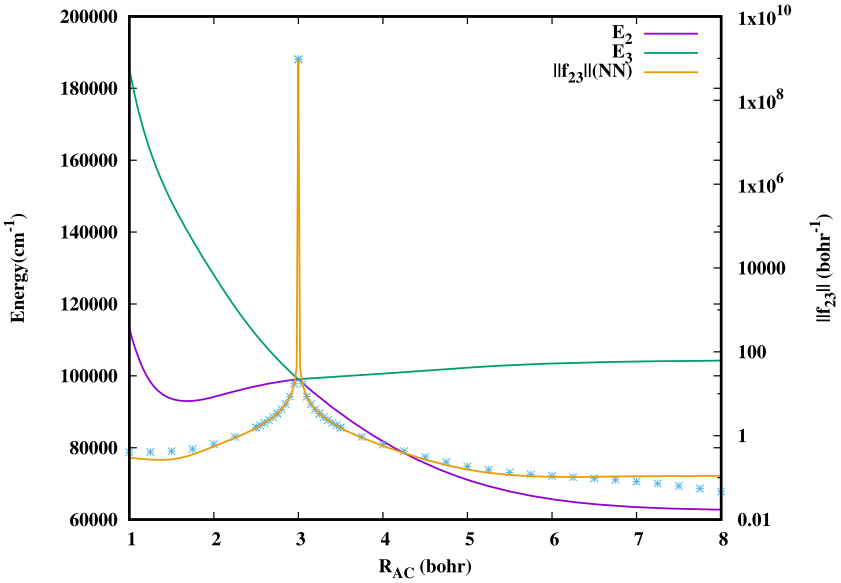

FIG. 4. Adiabatic energies of $2^1A'$ and $3^1A'$, and derivative coupling norm $\|\mathbf{f}_{23}\|$ as functions of R_{AC} (R_{AB} = 3.0 bohr and $\angle BAC = 60°$). Potential energy curves are shown in green ($3^1A'$) and purple ($2^1A'$) solid lines. *Ab initio* derivative coupling norms are shown as symbols, and the yellow solid line is the corresponding NN determined norm.

B. Reproduction of adiabatic energies

Two critical points have been identified on the ground state, including the D_{3h} minimum (minD_{3h}) and a collinear saddle point (sad$D_{\infty h}$). The corresponding *ab initio* determined and NN model determined energies and geometries are listed in Table II. As can be seen, the NN model determined and *ab initio* determined geometries are in excellent agreement: the geometries are almost identical. The point group symmetries of critical points are also strictly preserved, which validates the correct CNPI symmetry established in the NN-based $\mathbf{H}^{\mathrm{d}}$ through Eq. (2). The energies of critical points are also well reproduced, with the errors being less than 50 cm^{-1}.

Figures 1–3 present three energy cuts as functions of ρ along different arrangements: D_{3h}, C_{2v}, and collinear. It is important to note that the fitting data do not include the corresponding *ab initio* energies. However, as can be seen from these figures, the NN-based $\mathbf{H}^{\mathrm{d}}$ reproduces these *ab initio* energies very well, validating its accuracy. In Fig. 1, conical intersections occur between the first excited state ($2^1A'$) and the second excited state ($3^1A'$) at D_{3h} geometries, forming a degenerate $^1E'$ state. At D_{3h} geometries, the off-diagonal elements of $\mathbf{H}^{\mathrm{d}}$ vanish ($x = 0$ and $y = 0$), then $E_1 = V_a^{(0)}$ and

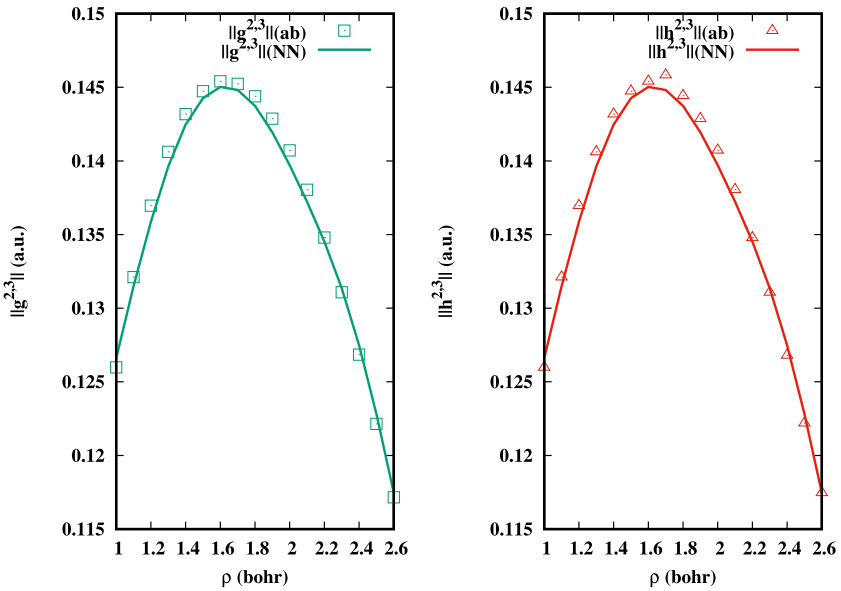

FIG. 5. The reproduction of $\|\mathbf{g}^{2,3}\|$ (left) and $\|\mathbf{h}^{2,3}\|$ (right). The *ab initio* $\|\mathbf{g}^{2,3}\|$ and $\|\mathbf{h}^{2,3}\|$ are shown as symbols, and the corresponding results from the NN-based $\mathbf{H}^{\mathrm{d}}$ are shown as solid lines.

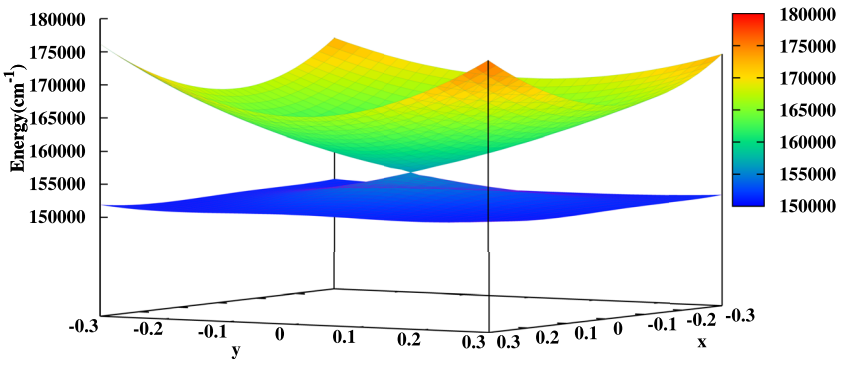

FIG. 6. Adiabatic potential energy surfaces for $2^1A'$ and $3^1A'$ states with fixed ρ = 1.65 bohr as functions of x and y.

$E_2 = E_3 = V_E^{(0)}$. Therefore, the $^1E'$ degeneracy is reproduced by the NN-based $\mathbf{H}^{\mathrm{d}}$. In Fig. 3, avoided crossing between $1^1A'$ and $2^1A'$ can be observed. Meanwhile, there is a cusp along the potential energy curve of $3^1A'$, which suggests a conical intersection between $3^1A'$ and a fourth state. Even though the current model does not include this fourth state, the *ab initio* energies were still reproduced with great accuracy, which demonstrates the powerful fitting ability of the NN-based ansatz.

C. Reproduction of derivative couplings and $^1E'$ state conical intersection seam

The most notable feature for H_3^+ system is the symmetry required $^1E'$ state conical intersection at D_{3h} geometries, where the derivative coupling $\mathbf{f}_{23}$ diverges. The fitting-and-diabatizing method is a derivative-based method, which aims to reproduce derivative couplings as accurately as possible. However, according to the theory,[4,73] the derivative couplings cannot be completely removed by an AtD transformation. Thus, the diabatization presented in this work minimizes the residual derivative coupling in the least squares sense. In other words, $\mathbf{H}^{\mathrm{d}}$ provides a removable approximation to the derivative couplings. Figure 4 examines the reproduction of $\|\mathbf{f}_{23}\|$ by NN-based $\mathbf{H}^{\mathrm{d}}$. There is a conical intersection at R_{AC} = 3.0 bohr. Since this conical intersection is required by symmetry, both *ab initio* and $\mathbf{H}^{\mathrm{d}}$ determined $\|\mathbf{f}_{23}\|$ exhibit an extremely sharp peak, showing the tendency to diverge. The rapid fall in $\|\mathbf{f}_{23}\|$ near the conical intersection is reproduced, which is essential for the description of the non-adiabatic transition facilitated by the conical intersection. Away from the conical intersection, there seem to be large discrepancies between *ab initio* and $\mathbf{H}^{\mathrm{d}}$ determined results. However, considering the logarithmic scaling of $\|\mathbf{f}_{23}\|$ and the divergent nature of derivative couplings, the differences can be regarded as being small.

The corresponding $^1E'$ state CI seam is defined by the equation s = 0. In the branching plane, which is perpendicular to the CI seam, the degeneracy is lifted in a linear manner near the vicinity of CI. The branching plane is defined by $\mathbf{g}$ (energy difference gradient) and $\mathbf{h}$ (interstate coupling gradient) vectors.[58] Thus, the reproduction of $\mathbf{g}$ and $\mathbf{h}$ is crucial for the description of the local topography of CI. Figure 5 exhibits the reproduction of $\mathbf{g}^{2,3}$ and $\mathbf{h}^{2,3}$ along the $^1E'$ CI seam (s = 0) by the NN-based $\mathbf{H}^{\mathrm{d}}$. As shown in the figure, the

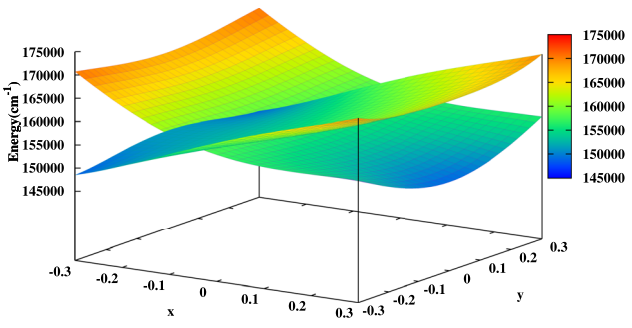

FIG. 7. H_{22}^{d} and H_{33}^{d} with fixed ρ = 1.65 bohr as functions of x and y.

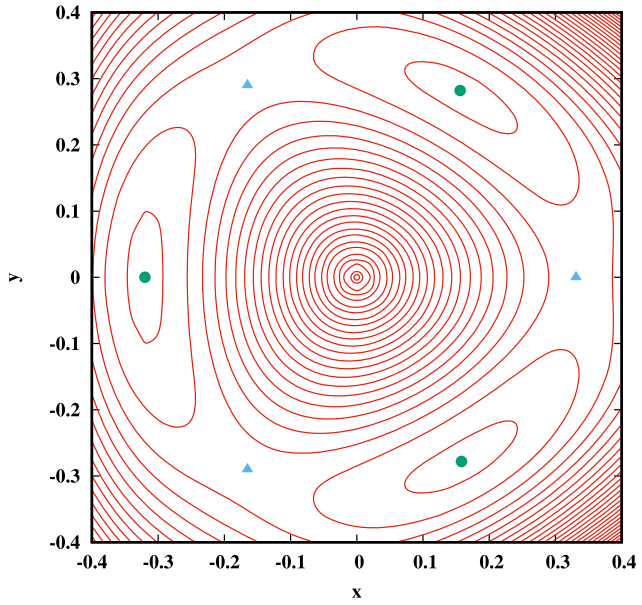

FIG. 8. Contour plot of $2^1A'$ adiabatic potential energy surface with fixed ρ = 1.65 bohr. Three minima are shown as dots, and three saddle points are shown as triangles.

norms of NN determined $\mathbf{g}^{2,3}$ and $\mathbf{h}^{2,3}$ are very close to the *ab initio* counterparts.

The lifting of a doubly degenerate electronic $^1E'$ state here is also an example of JT effects. In the case of H_3^+, it is an $E \otimes e$ JT system, where x and y constitute the doubly degenerate vibrational e mode. Figure 6 displays the NN determined adiabatic potential energy surfaces for $2^1A'$ and $3^1A'$ states with fixed $\rho = 1.65$ bohr. The $^1E'$ conical intersection at $x = y = 0$ is clearly demonstrated. Correspondingly, Fig. 7 shows the diabatic matrix elements $\mathbf{H}^{\mathrm{d}}_{22}$ and $\mathbf{H}^{\mathrm{d}}_{33}$, which exhibit no cusps and intersect properly. In JT systems, with the degeneracy lifted, the system can be stabilized via forming local minima. Figure 8 shows the contour plot of NN determined adiabatic PES for the $2^1A'$ state on the same grid. The PES clearly shows three minima, separated by three saddle points, which are observed in the $E \otimes e$ JT systems.

All these results demonstrate that the NN-based $\mathbf{H}^{\mathrm{d}}$ can describe the $^1E'$ state conical intersection seam and its local topography very accurately.

IV. SUMMARY

The PIP-NN approach is introduced to the construction of diabatic ansatz for the $(E + A) \times (e + a)$ Jahn–Teller and Pseudo-Jahn–Teller systems. It is based on the polynomial expansion of Viel and Eisfeld, the coefficients of which are expressed with NN functions that take PIPs as input. This PIP-NN-based diabatic ansatz not only preserves the correct CNPI symmetry but also provides NN functional flexibility to accurately reproduce the *ab initio* electronic structure data. Compared to the work of Williams, Eisfeld, and co-workers,[37–40] the present PIP-NN based approach provides a more flexible and compact NN-based diabatic ansatz. The PIP-NN-based ansatz is applied to the ZY fitting-and-diabatizing procedure for the H_3^+ system and results in excellent quality. The *ab initio* energies and energy gradients have been reproduced with satisfactory accuracy. The behavior of the derivative couplings near conical intersection seam agrees well with *ab initio* data, thus preventing artificially diabolical singularities.[74] The PIP-NN-based diabatic ansatz can also provide an accurate description of the local topology of the $^1E'$ state conical intersection, as evinced by the well-reproduced **g** and **h** vectors and the local minima due to the JT effect.

H_3^+ is a very simple example of JT or PJT systems, which only has three internal degrees of freedom. However, the idea of expressing the coefficients of symmetric polynomial expansion with NN(PIP) functions can be readily applied to other more complicated types of JT and PJT systems.[32,35,36,60,75–77] For example, Eisfeld and co-workers developed a diabatic ansatz based on polynomial expansion for the $^2E''$ first excited state of NO_3,[32] which can easily incorporate NN(PIP). The six internal degrees of freedom of NO_3 were decomposed into s_1, s_2, s_3 $(\mathfrak{s}_{3x}, \mathfrak{s}_{3y})$, and s_4 $(\mathfrak{s}_{4x}, \mathfrak{s}_{4y})$, where s_1 transforms as a_1', s_2 transforms as a_2'', and s_3 and s_4 transform as e'. Each DPEM element can be broken down according to the coordinates involved and the order of the polynomials, the diagonal element in Eq. (10) of Ref. 32, for instance. In this equation, the terms that only involve s_1 or s_2, such as $V_a(s_1)$, $V_b(s_2)$, and $V_{ab}(s_1, s_2)$, can be simply expressed by a NN(PIP), since s_1 and s_2 are invariant under the $\widehat{C}_3$ operation. The terms that mix s_1, s_2 and s_3, s_4, $V_{abee}(s_1, s_2, \mathfrak{s}_{3x}, \mathfrak{s}_{3y}, \mathfrak{s}_{4x}, \mathfrak{s}_{4y})$, for example, can then be written as $\mathrm{NN(PIP)} \cdot V_{ee}(\mathfrak{s}_{3x}, \mathfrak{s}_{3y}, \mathfrak{s}_{4x}, \mathfrak{s}_{4y})$, where V_{ee} is the symmetric polynomials involving two e' modes. As can be seen, the NN(PIP) is introduced to absorb the dependence of DPEM on s_1 and s_2. For other DPEM elements, NN(PIP) can be introduced in a similar manner.

To conclude, a flexible and compact PIP-NN-based diabatic ansatz for systems with non-Abelian systems is proposed. It is based on the symmetric polynomial expansion of Viel and Eisfeld, the coefficients of which are expressed with NN functions that take PIPs as input. Therefore, the present work completes the PIP-NN based representation of DPEM with correct symmetries. In combination with ZY fitting-and-diabatizing method, we hope this PIP-NN based diabatic ansatz will enable us to accurately diabatize even more complicated systems with non-Abelian symmetries, thus facilitating the study of non-adiabatic processes in JT and PJT systems.

ACKNOWLEDGMENTS

This work was supported by the U.S. Department of Energy (Grant No. DE-SC0015997 to D.R.Y.) and the National Natural Science Foundation of China (Grant No. 22288201 to D.H.Z.).

AUTHOR DECLARATIONS

Conflict of Interest

The authors have no conflicts to disclose.

Author Contributions

Yafu Guan: Software (lead); Visualization (lead); Writing – original draft (lead). **David R. Yarkony:** Conceptualization (equal); Methodology (equal); Writing – review and editing (equal). **Dong H. Zhang:** Conceptualization (equal); Methodology (equal); Writing – review and editing (equal).

DATA AVAILABILITY

The data that support the findings of this study are available from the corresponding author upon reasonable request.

REFERENCES

[1] M. A. Robb, *Theoretical Chemistry for Electronic Excited States* (Royal Society of Chemistry, 2018), Vol. 12.
[2] Y. Guan, C. Xie, D. R. Yarkony, and H. Guo, Phys. Chem. Chem. Phys. **23**, 24962 (2021).
[3] M. Baer, Chem. Phys. **15**, 49 (1976).
[4] C. A. Mead and D. G. Truhlar, J. Chem. Phys. **77**, 6090 (1982).
[5] M. Baer, Phys. Rep. **358**, 75 (2002).
[6] R. Abrol and A. Kuppermann, J. Chem. Phys. **116**, 1035 (2002).
[7] R. G. Sadygov and D. R. Yarkony, J. Chem. Phys. **109**, 20 (1998).
[8] C. R. Evenhuis and M. A. Collins, J. Chem. Phys. **121**, 2515 (2004).
[9] C. R. Evenhuis, X. Lin, D. H. Zhang, D. Yarkony, and M. A. Collins, J. Chem. Phys. **123**, 134110 (2005).
[10] O. Godsi, C. R. Evenhuis, and M. A. Collins, J. Chem. Phys. **125**, 104105 (2006).
[11] Z. Xu, M. Baer, and A. J. C. Varandas, J. Chem. Phys. **112**, 2746 (2000).
[12] S. Ghosh, S. Mukherjee, B. Mukherjee, S. Mandal, R. Sharma, P. Chaudhury, and S. Adhikari, J. Chem. Phys. **147**, 074105 (2017).
[13] G. W. Richings and G. A. Worth, J. Phys. Chem. A **119**, 12457 (2015).

[14]R. J. Cave and M. D. Newton, Chem. Phys. Lett. **249**, 15 (1996).
[15]R. J. Cave and M. D. Newton, J. Chem. Phys. **106**, 9213 (1997).
[16]H. J. Werner and W. Meyer, J. Chem. Phys. **74**, 5802 (1981).
[17]C. Petrongolo, G. Hirsch, and R. J. Buenker, Mol. Phys. **70**, 825 (1990).
[18]A. J. Dobbyn and P. J. Knowles, Mol. Phys. **91**, 1107 (1997).
[19]C. E. Hoyer, X. Xu, D. Ma, L. Gagliardi, and D. G. Truhlar, J. Chem. Phys. **141**, 114104 (2014).
[20]C. E. Hoyer, K. Parker, L. Gagliardi, and D. G. Truhlar, J. Chem. Phys. **144**, 194101 (2016).
[21]K. Ruedenberg and G. J. Atchity, J. Chem. Phys. **99**, 3799 (1993).
[22]G. J. Atchity and K. Ruedenberg, Theor. Chem. Acc. **97**, 47 (1997).
[23]T. Pacher, L. S. Cederbaum, and H. Köppel, J. Chem. Phys. **89**, 7367 (1988).
[24]T. Pacher, C. A. Mead, L. S. Cederbaum, and H. Köppel, J. Chem. Phys. **91**, 7057 (1989).
[25]T. Pacher, H. Köppel, and L. S. Cederbaum, J. Chem. Phys. **95**, 6668 (1991).
[26]D. Simah, B. Hartke, and H.-J. Werner, J. Chem. Phys. **111**, 4523 (1999).
[27]H. Köppel, W. Domcke, and L. S. Cederbaum, "Multimode molecular dynamics beyond the Born-Oppenheimer approximation," in *Advances in Chemical Physics* (John Wiley & Sons, Ltd., 1984), Chap. II, pp. 59–246.
[28]A. Viel and W. Eisfeld, J. Chem. Phys. **120**, 4603 (2004).
[29]W. Eisfeld and A. Viel, J. Chem. Phys. **122**, 204317 (2005).
[30]A. Viel, W. Eisfeld, S. Neumann, W. Domcke, and U. Manthe, J. Chem. Phys. **124**, 214306 (2006).
[31]S. Faraji, H. Köppel, W. Eisfeld, and S. Mahapatra, Chem. Phys. **347**, 110 (2008).
[32]W. Eisfeld, O. Vieuxmaire, and A. Viel, J. Chem. Phys. **140**, 224109 (2014).
[33]A. V. Marenich and J. E. Boggs, J. Chem. Phys. **122**, 024308 (2005).
[34]A. V. Marenich and J. E. Boggs, Chem. Phys. Lett. **404**, 351 (2005).
[35]D. Opalka and W. Domcke, Chem. Phys. Lett. **494**, 134 (2010).
[36]D. Opalka and W. Domcke, J. Chem. Phys. **132**, 154108 (2010).
[37]D. M. G. Williams and W. Eisfeld, J. Chem. Phys. **149**, 204106 (2018).
[38]D. M. G. Williams, A. Viel, and W. Eisfeld, J. Chem. Phys. **151**, 164118 (2019).
[39]D. M. G. Williams and W. Eisfeld, J. Phys. Chem. A **124**, 7608 (2020).
[40]A. Viel, D. M. G. Williams, and W. Eisfeld, J. Chem. Phys. **154**, 084302 (2021).
[41]N. Wittenbrink, F. Venghaus, D. Williams, and W. Eisfeld, J. Chem. Phys. **145**, 184108 (2016).
[42]X. Zhu and D. R. Yarkony, J. Chem. Phys. **132**, 104101 (2010).
[43]X. Zhu and D. R. Yarkony, J. Chem. Phys. **136**, 174110 (2012).
[44]X. Zhu and D. R. Yarkony, J. Chem. Phys. **137**, 22A511 (2012).
[45]X. Zhu and D. R. Yarkony, J. Chem. Phys. **140**, 024112 (2014).
[46]P. R. Bunker and P. Jensen, *Molecular Symmetry and Spectroscopy* (NRC Research Press, 2006).
[47]T. Lenzen and U. Manthe, J. Chem. Phys. **147**, 084105 (2017).
[48]T. Lenzen, W. Eisfeld, and U. Manthe, J. Chem. Phys. **150**, 244115 (2019).
[49]B. J. Braams and J. M. Bowman, Int. Rev. Phys. Chem. **28**, 577 (2009).
[50]C. Xie, X. Zhu, D. R. Yarkony, and H. Guo, J. Chem. Phys. **149**, 144107 (2018).
[51]Y. Guan, H. Guo, and D. R. Yarkony, J. Chem. Phys. **150**, 214101 (2019).
[52]B. Jiang and H. Guo, J. Chem. Phys. **139**, 054112 (2013).
[53]J. Li, B. Jiang, and H. Guo, J. Chem. Phys. **139**, 204103 (2013).
[54]K. Shao, J. Chen, Z. Zhao, and D. H. Zhang, J. Chem. Phys. **145**, 071101 (2016).
[55]B. Jiang and H. Guo, J. Chem. Phys. **141**, 034109 (2014).
[56]D. H. Zhang and H. Guo, Annu. Rev. Phys. Chem. **67**, 135 (2016).
[57]B. Fu, X. Shan, D. H. Zhang, and D. C. Clary, Chem. Soc. Rev. **46**, 7625 (2017).
[58]D. R. Yarkony, Acc. Chem. Res. **31**, 511 (1998).
[59]T. C. Thompson, D. G. Truhlar, and C. A. Mead, J. Chem. Phys. **82**, 2392 (1985).
[60]S. Bhattacharyya, D. Opalka, L. V. Poluyanov, and W. Domcke, J. Phys. Chem. A **118**, 11962 (2014).
[61]H. Kamisaka, W. Bian, K. Nobusada, and H. Nakamura, J. Chem. Phys. **116**, 654 (2002).
[62]L. P. Viegas, A. Alijah, and A. J. C. Varandas, J. Chem. Phys. **126**, 074309 (2007).
[63]S. Mukherjee, D. Mukhopadhyay, and S. Adhikari, J. Chem. Phys. **141**, 204306 (2014).
[64]Z. Yin, B. J. Braams, B. Fu, and D. H. Zhang, J. Chem. Theory Comput. **17**, 1678 (2021).
[65]T. C. Thompson, G. Izmirlian, S. J. Lemon, D. G. Truhlar, and C. A. Mead, J. Chem. Phys. **82**, 5597 (1985).
[66]K. Hornik, M. Stinchcombe, and H. White, Neural Netw. **2**, 359 (1989).
[67]A. Pukrittayakamee, M. Malshe, M. Hagan, L. M. Raff, R. Narulkar, S. Bukkapatnum, and R. Komanduri, J. Chem. Phys. **130**, 134101 (2009).
[68]Y. Guan, D. H. Zhang, H. Guo, and D. R. Yarkony, Phys. Chem. Chem. Phys. **21**, 14205 (2019).
[69]M. T. Hagan and M. B. Menhaj, IEEE Trans. Neural Netw. **5**, 989 (1994).
[70]H. Lischka, R. Shepard, R. M. Pitzer, I. Shavitt, M. Dallos, T. Müller, P. G. Szalay, M. Seth, G. S. Kedziora, S. Yabushita, and Z. Zhang, Phys. Chem. Chem. Phys. **3**, 664 (2001).
[71]H. Lischka, M. Dallos, P. G. Szalay, D. R. Yarkony, and R. Shepard, J. Chem. Phys. **120**, 7322 (2004).
[72]Z. Xie and J. M. Bowman, J. Chem. Theory Comput. **6**, 26 (2010).
[73]M. Baer, *Beyond Born-Oppenheimer: Electronic Nonadiabatic Coupling Terms and Conical Intersections* (John Wiley & Sons, 2006).
[74]X. Zhu and D. R. Yarkony, J. Phys. Chem. A **119**, 12383 (2015).
[75]T. Weike, D. M. G. Williams, A. Viel, and W. Eisfeld, J. Chem. Phys. **151**, 074302 (2019).
[76]M. A. Collins, O. Godsi, S. Liu, and D. H. Zhang, J. Chem. Phys. **135**, 234307 (2011).
[77]Y. Shu, J. Kryven, A. G. Sampaio de Oliveira-Filho, L. Zhang, G.-L. Song, S. L. Li, R. Meana-Pañeda, B. Fu, J. M. Bowman, and D. G. Truhlar, J. Chem. Phys. **151**, 104311 (2019).